

Electroconductance oscillations and quantum interference in ballistic nanostructures

Yong S. Joe and Sergio E. Ulloa

*Department of Physics and Astronomy and Condensed Matter and Surface Sciences Program,
Ohio University, Athens, Ohio 45701-2979*

(Received 9 June 1992; revised manuscript received 30 November 1992)

We report theoretical studies of a quantum-interference phenomenon in ballistic nanometer-size constrictions analogous to the electrostatic Aharonov-Bohm effect. Modulating an applied-potential step V_T in one of the branches of a multiply connected system allows the observation of conductance oscillations, even in the absence of magnetic fields, as they are produced by quantum-interference between voltage-shifted states in the different branches. Electric depopulation of subbands can also be seen at larger V_T . We show that these aperiodic oscillations are strong for realistic structural parameters, robust against increasing temperature, and compare well with the expected phase changes in a simple single-channel model.

A number of quantum phase-interference effects in electronic transport have been studied intensively in recent years. A prime example of these phenomena is the magnetic Aharonov-Bohm (AB) effect;¹ a manifestation of the phase shifts of electronic wave functions produced by magnetic vector potentials. This effect has been studied extensively in solid-state systems in normal-metal rings² and cylinders,³ and in rings patterned onto high-mobility GaAs-Al_xGa_{1-x}As semiconductor heterojunctions.^{4,5} Experimental and theoretical work has shown that resistance oscillations are observed in the magnetic AB effect due to quantum interference between two or more inequivalent paths enclosing a varying magnetic flux. On the other hand, wave-function phase shifts and the ensuing interference between two classical paths may also be produced by the application of a potential difference between the pathways (the *electrostatic* AB effect¹). Variations of electrostatic AB experiments have been proposed by Boyer and others⁶ to exhibit the relationship between a semiclassical lag effect — due to electrostatic fields acting on electrons passing along different paths — and the unique quantum-interference phase shifts induced even in the absence of force on the electrons.¹ Diffraction experiments have also been performed by Matteucci and co-workers,⁶ who studied electron beams traversing a bimetallic wire, where the contact potential difference between the components produced quantum phase-shifting effects. Quantum-interference “devices” in solids, showing conductance oscillations controlled by external potentials, have been proposed in the literature,^{4,7} and several structures have been fabricated. Washburn *et al.* studied the effects of transverse electric fields in small ($\approx 1 \mu\text{m}$) metallic loops,⁸ de Vegvar *et al.* presented results for rings defined on GaAs-Al_xGa_{1-x}As using narrow metal gates,⁹ and Yacoby *et al.* used a double-gate geometry in a high-mobility semiconductor system.¹⁰ These experiments have demonstrated that applied electric fields can indeed modulate the sample resistance by shifting the phases of the wave functions, by either a lag or an AB effect. However, a detailed analysis of the experimental observations was complicated by remnant impurity scat-

tering and multiple conducting channels,^{8,9} results that have perhaps discouraged further experiments.

In this paper, we report calculations of conductance oscillations in quantum ballistic narrow channels produced by modulating an applied transverse potential V_T along one of the branches of a multiply connected region. We show that this geometry — similar to that of Ref. 9, although fully in the ballistic regime (such that the elastic mean free path and the phase-coherence length are much larger than the size of the structure¹¹) — allows the observation of conductance oscillations even in the presence of multiple conducting channels and the geometrical backscattering effects fully incorporated in our calculations. These aperiodic oscillations arise as a quantum-interference effect between phase-shifted branches of the wave function in the structure, similar to the lag effects described by Boyer.⁶ We show that the number of conductance oscillations increases with barrier length l , as expected from simple considerations, and that the modulation is fairly robust against increasing temperature. In addition, we show that the applied potential can produce strong modulation of the conductance for realistic structural-parameter values, suggesting the possible observation of this effect in the ballistic multiple-channel regime, and which we hope would promote experiments in these systems.

The type of structure used in our calculations is shown schematically in Fig. 1(a), where relevant parameters are defined. By depositing a rectangular infinite-repulsive potential obstacle in the center of a narrow constriction (such as those described in Ref. 12, for example), the wave function of the incident electron is forced to “split” into two paths before it recombines at the other end of the channel. The ballistic electron conduction within the bifurcated channel is locally influenced by a potential barrier V_T along the top branch of the structure. For simplicity, most of the results presented here assume that the applied transverse potential barrier V_T has sharp edges at the ends of its length l , although this has no qualitative effect in what follows [as calculations with rounded potentials give similar results — see Fig. 3(a) below]. Figure 1(b) shows a cross section of the po-

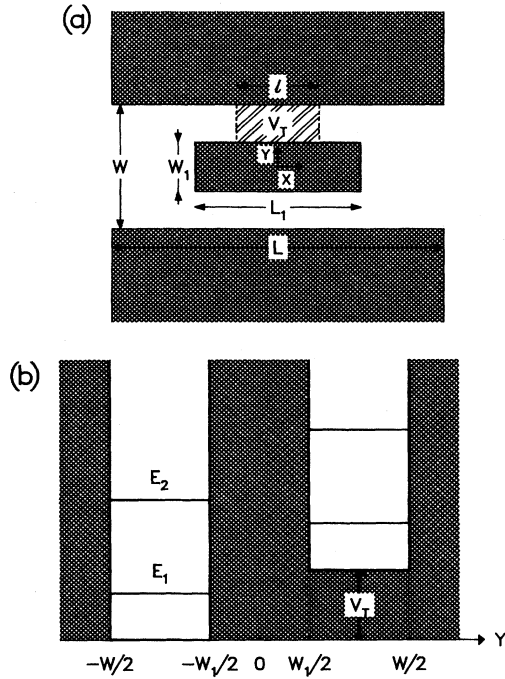


FIG. 1. (a) Schematic illustration of the geometry studied. The top branch is modulated by an applied transverse potential V_T . (b) Cross section through $x = 0$ showing potential and energy subbands. Cross-hatched areas are forbidden for electrons.

tential along the $x = 0$ line in the region of the barrier (centered at the origin).

In order to investigate the conductance of such structures, we describe the wave motion along the structure (x direction) by a nearest-neighbor tight-binding Hamiltonian in a lattice with periodicity a much smaller than the electronic wavelength λ ($\lambda \gg a \approx 5 \text{ \AA}$). The hopping amplitude t between lattice sites is determined from the effective mass of the carrier in the heterostructure ($m = 0.067m_e$ in GaAs), and is then given by $t = \hbar^2/2ma^2$. On the other hand, in each region with straight walls parallel to the x axis, the confinement potential $V_c(y)$ in the y direction gives rise to a set of subbands E_n such that

$$\left\{ -\frac{\hbar^2}{2m} \frac{d^2}{dy^2} + V_c(y) \right\} \phi_n(y) = E_n \phi_n(y), \quad (1)$$

where $V_c(y) = 0$, except for the regions defined by hard walls [where it is infinite, and shown as cross-hatched regions in Fig. 1(a)], and in the region with the finite barrier, where $V_c(y) = V_T$ for $W \geq 2y \geq W_1$. We have employed a modular recursive Green's-function method to couple the transverse modes in the different regions,¹³ which allows the calculation of scattering amplitudes for this and any geometry. The conductance G is evaluated from the Landauer formula for a two-terminal configuration,¹⁴ $G = (2e^2/h)\text{Tr}(\mathbf{t}\mathbf{t}^\dagger) = (2e^2/h)\sum_{n,m} |t_{nm}|^2$, where \mathbf{t} is the matrix (with element t_{nm}) of transmission probability amplitudes at the Fermi energy (from

subband m at one reservoir to subband n at the other).

The transverse energy levels on both branches of the impenetrable central obstacle are obviously degenerate when $V_T = 0$, but separate linearly with the external potential [i.e., $E_n \rightarrow E_n + V_T$ in the top branch, see Fig. 1(b)]. At a fixed Fermi energy E_F , increasing the barrier voltage leads to the eventual electric depopulation of subbands on the branch with the barrier (top), as the subband energy exceeds E_F . In what follows, all energies are normalized with respect to the first subband in the constriction, $E_1^0 = \hbar^2\pi^2/2mW^2$.

The conductance of the structure $G(V_T)$, normalized to $G_0 = G(V_T = 0)$, is shown in Fig. 2 for different scaled values of the Fermi energy, $\tilde{E}_F = (E_F/E_1^0)^{1/2}$. Curves are offset vertically for clarity. Conductance oscillations induced by a changing potential $\tilde{V}_T = (V_T/E_1^0)^{1/2}$ are clearly seen for all values of \tilde{E}_F displayed, *regardless* of the number of current-carrying states in each channel (a number of evanescent states — typically 25 — are included in the calculation to guarantee fully convergent solutions). At the lowest \tilde{E}_F shown ($= 4.1$) there is only one propagating mode in *each* branch of the structure for $\tilde{V}_T = 0$. As \tilde{V}_T increases, the top branch subband depopulates until it no longer transmits for $\tilde{V}_T > 3.4$. The conductance then drops to its nonoscillating minimum (given by the still propagating mode in the bottom branch of the structure), since branch interference is no longer possible. The rather strong oscillations in G versus \tilde{V}_T can then be seen as the interference of two paths, where \tilde{V}_T induces a phase lag in the top-branch wave function, with respect to that in the bottom branch. Moreover, as we discuss below, intersubband scattering and multiple reflections do not severely affect this picture. However, one would expect these effects to be more important as \tilde{E}_F

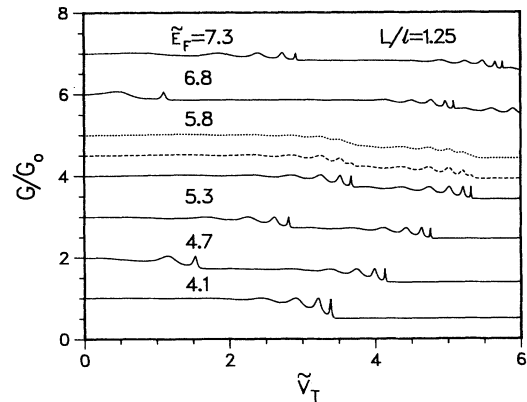


FIG. 2. Conductance ratio G/G_0 vs $\tilde{V}_T = (V_T/E_1^0)^{1/2}$ for different values of $\tilde{E}_F = (E_F/E_1^0)^{1/2}$, and fixed l . Curves are vertically offset one unit for clarity. Nonoscillatory traces at the bottom right reflect total subband depopulation in the top branch. Solid, dashed, and dotted curves for $\tilde{E}_F = 5.8$ show temperature dependence of G for $kT/E_1^0 = 0, 0.01$, and 0.02 , respectively (corresponding to 0, 2, and 4 K, approximately). Smearing of oscillations is appreciable at the highest T , but negligible at $T \approx 1$ K.

increases, since intersubband scattering between multiple current-carrying states is appreciable. Nevertheless, even for $\tilde{E}_F = 6.8$ and 7.3 (topmost curves in Fig. 2, when *three* modes carry current in each branch at $\tilde{V}_T = 0$), the oscillations in G are still strong, in between successive jumps produced by the depopulation of channels. For other \tilde{E}_F values shown (4.7, 5.3, and 5.8), the conductance curve has basically the same features, except that there are two propagating modes in each channel. Consequently, conductance oscillations arising from the second propagating subband can be seen between $\tilde{V}_T \approx 1$ and 3.5 , and are shifted upwards for higher \tilde{E}_F .

This phase-lag mechanism explains the conductance modulations in Fig. 2, as well as the persistence of conductance modulation for smoother potential barriers [if only with somewhat smaller amplitudes, see Fig. 3(a)]. It is also clear that it is possible to induce a phase lag *with-*

out a barrier V_T if only the *width* of one of the branches is modulated. Since the branch width determines the position of the energy subbands there, its variation produces an effective varying barrier for the propagating modes, which in turn yields conductance oscillations. The additional experimental challenge in this “simpler” geometry is of course the ability to fabricate a gate with separate “side controls,” examples of which already exist.¹² (Our theoretical results on this nonbarrier asymmetric geometry will be presented elsewhere.)

The features of the electroconductance oscillations would naturally be expected to depend on the path length l over which the external potential V_T is applied. Figure 3(a) demonstrates this length dependence on the conductance oscillations, showing the conductance ratio G/G_0 at a fixed $\tilde{E}_F = 5.3$, as a function of \tilde{V}_T and for different l values. As l is varied (while keeping both L and L_1 fixed — see Fig. 1), both the position and amplitude of the conductance peaks change. For smaller l values [top traces in Fig. 3(a)], consecutive peaks (given by $\Delta\Phi = 2\pi n$, where n is an integer) require a larger change in \tilde{V}_T , in accordance with the simple model described by Eq. (2) below. Notice also that oscillations become sharper for larger l values, as the constructive interference condition is more precariously achieved. We should also point out that the variation of the obstacle length L_1 for a fixed l has no noticeable effect on these oscillations (not shown here), demonstrating that it is the modulation by V_T and not the bifurcation itself which defines the conductance features. (The situation changes naturally, however, in the nonbarrier asymmetric geometry discussed above, where the entire branch length determines the phase lag.) For smooth potential edges, electroconductance oscillations due to changes in V_T are also seen [dashed curve in Fig. 3(a)], if only with a smaller peak-to-valley ratio. Here, the potential barrier is gradually ramped over 0.1 of its length on each end, making an effectively shorter step which shows shallower features. For an even smoother potential, so that the step reaches its highest value of V_T only over the central one-tenth of its length, the oscillations are basically smeared out, and only slow depopulation transitions are seen (dotted line).

One may use simple considerations to analyze the phase changes suffered by the electron traversing the obstacle region. The “electrostatic” phase difference $\Delta\Phi$ between the two paths induced by V_T is given by $\Delta\Phi = V_T\tau/\hbar = mV_Tl/\hbar^2k_x$,^{1,4,6} where τ is the traversal time through the barrier region, and k_x is the electronic wave number in this region along the x direction, $k_x = [2m(E_F - E_n - V_T)/\hbar^2]^{1/2}$. Here, $E_n + V_T$ is the subband energy in the *top* branch of the structure closest to E_F from below. The phase shift $\Delta\Phi$ between the two contiguous paths can then be written as

$$\Delta\Phi = \frac{\pi l}{2W} \frac{\tilde{V}_T^2}{[\tilde{E}_F^2 - E_n/E_1^0 - \tilde{V}_T^2]^{1/2}}. \quad (2)$$

This single-mode expression clearly neglects intermode mixing and backscattering effects, typically present in

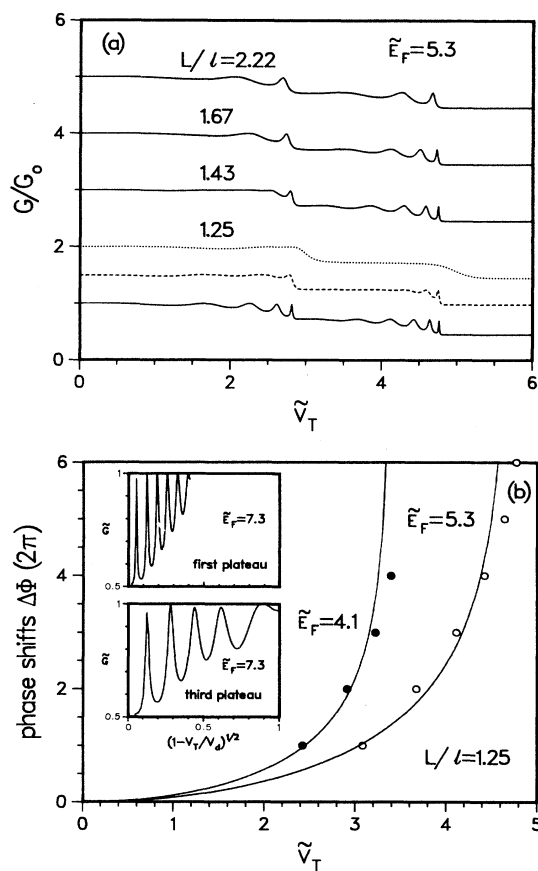


FIG. 3. (a) Barrier length dependence of G/G_0 vs \tilde{V}_T for $\tilde{E}_F = 5.3$. Shallower peaks in conductance are shown as length l decreases (top traces). Dashed and dotted lines: a smooth potential step ($L/l = 1.25$) also produces shallower features (see the text). (b) Predicted [solid lines, Eq. (2)] and calculated (dots, Fig. 2) phase shifts $\Delta\Phi$ vs \tilde{V}_T . $\tilde{E}_F = 4.1$ for the left curve (\bullet), and $\tilde{E}_F = 5.3$ for the right curve (\circ). $L/l = 1.25$ is kept fixed. Insets show normalized conductance curves vs V_T measured with respect to the depopulation voltage value, V_d .

the structure (and included in the calculations of Fig. 2). The phase shifts in Eq. (2) for the different modes would superimpose *and* mix with others to produce oscillations in the real conductance curves. However, if only one mode is assumed to produce the interference peaks in G , one can examine the different features and compare with Eq. (2), as follows.

By examining the peak separation of the electroconductance oscillations for different Fermi energies, we confirm that the quantum-interference phase shifts modulated by \tilde{V}_T produce the oscillations in the conductance. Figure 3(b) shows the comparison between the predicted phase changes in Eq. (2) (solid lines) and the calculated peak positions in Fig. 2 (circles), indicating constructive interference between two alternative paths. The solid curves in Fig. 3(b) fit the calculated phase shifts within 5% over the range of $\tilde{V}_T \approx 2-5$. Notice that in this range, for both \tilde{E}_F values shown, there is only one populated subband in the top branch of the structure, to facilitate the comparison with the simple one-channel model. This good agreement indicates that backscattering and inter-channel mixing effects are not considerable, as they account for only the small deviations in Fig. 3(b). The agreement for higher E_F values slowly deteriorates, as expected for the multiple-channel regime.

Figure 3(b) also shows plots of the plateau conductances versus the barrier height, but measured from the "depletion" value at which the given transverse mode in the barrier region is depopulated. The conductance peaks then appear nearly periodic in terms of this "effective kinetic wave number" variable, as discussed before by Yacoby *et al.*¹⁰ for the one-mode case. Notice here, however, that this near-periodicity is also observed for high values of the Fermi energy, when several transverse modes are involved.

Finally, the low-temperature dependence of the electroconductance oscillations may be estimated from the

$T = 0$ behavior using the relation $G(E_F, V_T, T) = \int G(E, V_T, 0) (-df/dE)dE$. This expression takes into account only the broadening of the Fermi function $f(E)$. Inelastic-scattering effects are neglected here due to the typical low temperatures of ballistic experiments. Sample results for different temperatures, $kT/E_1^0 = 0.01$ and 0.02 , are shown in Fig. 2 as dashed and dotted curves, respectively, for $\tilde{E}_F = 5.8$. The oscillations in the electroconductance are suppressed at higher temperatures, although they persist fairly strong up to $kT \approx 0.01E_1^0 \approx 2$ K without much change. This is also a promising result for possible experimental observations. We should point out that our calculations predict large peak-to-valley ratios, as shown in Figs. 2 and 3 here (≈ 2 to 1 with about three populated channels), using realistic values for the different lengths and energies in the problem.^{11,12}

In conclusion, we have studied quantum-interference effects in transport, analogous to the electrostatic AB effect, in ballistic nanoconstrictions. Distinct features of the electroconductance oscillations include a strong dependence on the applied transverse potential V_T and barrier length l . The good agreement between the calculated phase shifts for the conductance oscillations and a simple one-channel model is evidence of quantum interference with voltage-shifted states without much strong-channel mixing being apparent. This effect should be observable in high-mobility semiconductor heterostructures in the ballistic regime. The observation of this phenomenon should be a challenge for experimentalists, and be an interesting complement to experiments reported to date in other systems.

We would like to thank Xiaoguang Wu for useful discussions. This work was supported by the U.S. Department of Energy under Grant No. DE-FG02-91ER45334. Calculations were performed on the Cray Y-MP at the Ohio Supercomputer Center.

¹Y. Aharonov and D. Bohm, Phys. Rev. **115**, 485 (1959).

²B. Pannetier *et al.*, Phys. Rev. Lett. **53**, 718 (1984); R. A. Webb *et al.*, *ibid.* **54**, 2696 (1985); V. Chandrasekhar *et al.*, *ibid.* **55**, 1610 (1985); S. Washburn and R. A. Webb, Adv. Phys. **35**, 375 (1986); F. P. Milliken *et al.*, Phys. Rev. Lett. **36**, 4465 (1987); A. D. Stone and Y. Imry, *ibid.* **56**, 189 (1986); Y. Isawa *et al.*, J. Phys. Soc. Jpn. **55**, 2523 (1986); J. K. Jain, Phys. Rev. Lett. **60**, 2074 (1988).

³D. Yu. Sharvin and V. Yu. Sharvin, Pis'ma Zh. Eksp. Teor. Fiz. **34**, 285 (1981) [JETP Lett. **34**, 272 (1981)]; B. L. Al'tshuler *et al.*, *ibid.* **35**, 476 (1982); [**35**, 588 (1982)]; M. Gijs *et al.*, Phys. Rev. Lett. **52**, 2069 (1984).

⁴S. Datta *et al.*, Phys. Rev. Lett. **55**, 2344 (1985).

⁵C. J. B. Ford *et al.*, J. Phys. Cond. Matt. **21**, L325 (1988); C. J. B. Ford *et al.*, Appl. Phys. Lett. **54**, 21 (1989); C. J. B. Ford *et al.*, Surf. Sci. **229**, 307 (1990).

⁶T. Boyer, Phys. Rev. B **8**, 1679 (1973); G. Matteucci and G. Pozzi, Phys. Rev. Lett. **54**, 2469 (1985).

⁷A. B. Fowler, US Patent No. 4,550,330 (29 October 1985);

S. Datta *et al.*, Appl. Phys. Lett. **48**, 487 (1986).

⁸S. Washburn *et al.*, Phys. Rev. Lett. **59**, 1791 (1987).

⁹P. de Vegvar *et al.*, Phys. Rev. B **40**, 3491 (1989).

¹⁰A. Yacoby *et al.*, Phys. Rev. Lett. **66**, 1938 (1991).

¹¹See, for example, C. W. J. Beenakker and H. van Houten, in *Solid State Physics*, edited by H. Ehrenreich, F. Seitz, and D. Turnbull (Academic, New York, 1991), Vol. 44, p. 1; S. E. Ulloa *et al.*, in *Handbook on Semiconductors*, edited by P. T. Landsberg (North-Holland, Amsterdam, 1992), p. 863.

¹²Y. Hirayama and T. Saku, Phys. Rev. B **42**, 11 408 (1990); S. W. Hwang *et al.*, *ibid.* **44**, 13 497 (1991).

¹³F. Sols *et al.*, J. Appl. Phys. **66**, 3892 (1989); S. Joe and S. E. Ulloa, MRS Ext. Abs. **EA-26**, 47 (1990).

¹⁴D. S. Fisher and P. A. Lee, Phys. Rev. B **23**, 6851 (1981); M. Büttiker, Phys. Rev. Lett. **57**, 1761 (1986); A. D. Stone and A. Szafer, IBM J. Res. Develop. **32**, 384 (1988); R. Landauer, J. Phys. Condens. Matter **1**, 8099 (1989).